

# Trends and Characteristics of High-Frequency Type II Bursts Detected by CALLISTO Spectrometers

A.C. Umuhire<sup>a</sup>, J. Uwamahoro<sup>b</sup>, K. Sasikumar Raja<sup>c</sup>, A. Kumari<sup>d</sup>, C. Monstein<sup>e</sup>

<sup>a</sup>*University of Rwanda, College of Science and Technology, Kigali, Rwanda  
(angelaciany@gmail.com)*

<sup>b</sup>*University of Rwanda, College of Education, Rwanda  
(mahorjpacis@gmail.com)*

<sup>c</sup>*Indian Institute of Astrophysics, II Block, Koramangala, Bengaluru - 560 034, India  
(sasikumar.raja@iiap.res.in)*

<sup>d</sup>*Department of Physics, University of Helsinki, P.O. Box 64, FI-00014 Helsinki, Finland  
(anshusingh628@gmail.com)*

<sup>e</sup>*Istituto Ricerche Solari (IRSOL), Università della Svizzera italiana (USI), CH-6605 Locarno-Monti, Switzerland  
(christian.monstein@irsol.usi.ch)*

---

## Abstract

Solar radio type II bursts serve as early indicators of incoming geo-effective space weather events such as coronal mass ejections (CMEs). In order to investigate the origin of high-frequency type II bursts (HF type II bursts), we have identified 51 of them (among 180 type II bursts from SWPC reports) that are observed by ground-based Compound Astronomical Low-cost Low-frequency Instrument for Spectroscopy and Transportable Observatory (CALLISTO) spectrometers and whose upper-frequency cutoff (of either fundamental or harmonic emission) lies in between 150 MHz-450 MHz during 2010 - 2019. We found that 60% of HF type II bursts, whose upper-frequency cutoff  $\geq$  300 MHz originate from the western longitudes. Further, our study finds a good correlation ( $\sim 0.73$ ) between the average shock speed derived from the radio dynamic spectra and the corresponding speed from CME data. Also, we found that analyzed HF type II bursts are associated with wide and fast CMEs located near the solar disk. In addition, we have analyzed the spatio-temporal characteristics of two of these high-frequency type II bursts and compared the derived from radio observations with those derived from multi-spacecraft CME observations from SOHO/LASCO and STEREO coronagraphs.

*Keywords:*

Radio bursts, Type II, Coronal Mass Ejections (CMEs)

---

*Email address:* angelaciany@gmail.com (A.C. Umuhire)

## 1. Introduction

Solar radio bursts (SRBs) in metric wavelengths, can be classified as i) type I bursts, which are usually associated with active regions (Elgaroy, 1977; Ramesh et al., 2013; Mercier et al., 2015); type II bursts, which are generally related with coronal shocks (Cane and Stone, 1984; Kumari et al., 2017c); iii) type III bursts, which are often associated with flares (Fainberg and Stone, 1970; Ratcliffe et al., 2014); iv) type IV bursts, generally associated with CMEs and flux ropes (Gary et al., 1985; Ramesh et al., 2004; Sasikumar Raja et al., 2014; Carley et al., 2017; Morosan et al., 2020; Kumari et al., 2021); and v) type V bursts, which often accompanies type III bursts (Stewart et al., 1965; Suzuki and Dulk, 1985). Type II radio bursts are slowly drifting and long-lasting (few minutes) in the solar dynamic spectra. They are believed to be plasma emission produced by a shock when it propagates through the solar corona (Mann et al., 1995; Zlotnik et al., 1998; Cliver et al., 2004; Schmidt et al., 2014). These bursts are often associated with the shock propagating ahead of a CME in the solar corona (e.g., Gopalswamy et al., 1998; Kumari et al., 2017a; Morosan et al., 2021; Majumdar et al., 2021). Type II bursts can sometimes occur without any CME, and are then associated with flares (Magdalenic et al., 2012; Su et al., 2015). Meter-wavelength type II bursts associated with CMEs can be used as a proxy to estimate the near-Sun kinematics and dynamics of a CME (Shanmugaraju et al., 2017; Kumari et al., 2017a,b). Type II bursts can also be observed in the decameter/hectometer (DH) frequency range ( $\leq 15$  MHz). There are various properties of meter/DH-wavelength type II radio burst, e.g. drift rates, frequency range, duration, etc., which can be used to study various properties of the ‘middle’ and/or ‘upper’ corona. While the meter-wavelength type II is of particular interest for CMEs near the Sun, the DH type IIs can indicate the presence of interplanetary CMEs (ICMEs; e.g., Mujiber Rahman et al., 2012; Vasanth and Umapathy, 2013). Hence, type II bursts can also act as an indicator of geomagnetic storms.

The starting frequency of the type II burst is often below 150 MHz, and its drift rate is  $\sim 0.3$  MHz/s (Maxwell and Thompson, 1962; Mann et al., 1995). The high starting frequency implies a radio source closer to the solar disk, hence crucial for space weather forecasting purposes (Makela et al., 2013). Several studies discussed the origin of type II bursts using different methods. For example, Gopalswamy et al. (2009a) used the leading edge method to show that the CME height at type II onset is similar to the height at the minimum of the Alfvén speed (Gopalswamy et al., 2001).

Ramesh et al. (2012) analyzed 41 type II bursts observed by the Gauribidanur Radioheliograph (GRAPH) at the Gauribidanur observatory and found that 92% of the bursts were located at or above the associated CME leading edge. Cho et al. (2013) used the 2011 February 13 high starting frequency type II burst to check if the associated CME generated it. They found that a CME driven shock can explain the origin of a type II burst in the low corona. Some other studies, e.g. Cane and Reames (1988) reported that almost all HF type II bursts are due to flares as their onset times often coincide with impulsive phases of flares. Vrsnak et al. (1995) reported about the time coincidence between the back-extrapolated onset time of type II bursts, with the peak energy release of the 28 high-frequency ( $> 273$  MHz) type II bursts. The idea was also supported by Shanmugaraju et al. (2009) who did an exclusive study on the source of the high ( $\geq 100$  MHz), low ( $\leq 50$  MHz) and middle ( $50 \text{ MHz} \leq f \leq 100 \text{ MHz}$ ) starting frequency type II bursts. Gopalswamy (2010) argued that all type II bursts are due to CMEs regardless of the wavelength.

Among these SRBs, the type II and type IV bursts are of special interest for space weather monitoring as they often occur in associations with coronal mass ejections (CMEs), solar flares (SFs), and solar energetic particles (SEPs) (Gosling et al., 1976; MacQueen, 1980; Gopalswamy et al., 1998; Kumari et al., 2019; Ndacyayisenga et al., 2021). CMEs, SFs, and SEPs are usually considered major space weather drivers (Cane and Reames, 1988; Reiner et al., 2000; Gopalswamy et al., 2010; Carley et al., 2020).

SEP events are due to the accelerated ions originating in large solar eruptions such as CMEs and solar flares (Gopalswamy, 2003). It is known that type II radio bursts are produced by electrons accelerated in MHD shocks. This implies a high degree of association between type II bursts and SEP events (Kahler et al., 1984a; Cane et al., 1990). Previous studies found a close relationship and association between DH type II bursts, SEP events with fast and wide CMEs Gopalswamy et al. (2002, 2003). The similar analysis by Lara et al. (2003) in the metric wavelength range (25 MHz to 625 MHz) confirmed that the trend extends to higher frequencies.

It is worth mentioning that after the launch of the WIND/WAVES (Bougeret et al., 1995), several similar studies that deal with the low-frequency SRBs observed by the radio receiver band-2 (RAD2) in the frequency range  $\approx 1 - 14$  MHz have been carried out (Bale et al., 1999; Gopalswamy,

2004a,b; Krupar et al., 2019; Gopalswamy et al., 2019). Note that such observations overlap with the field-of-view (FOV) of the Solar and Heliospheric Observatory (SOHO) mission’s Large Angle and Spectrometric Coronagraphs (LASCO; Brueckner et al., 1995).

The recent analysis by Umuhire et al. (2021) considered higher starting frequency to check whether the universal drift rate-frequency relationship extends to higher frequencies. They analyzed 128 type II radio bursts and emphasized on the 40 higher-starting-frequency bursts. The study compared two populations, type II bursts with the starting frequency less than 150 MHz and those with starting frequency greater or equal to 150 MHz. The radio burst data were obtained from different ground spectrometers, covering the period from 2010 to 2016.

Our current study is a statistical analysis of 51 type II bursts whose upper-frequency cut-off lies in between 150 MHz and 450 MHz, observed by a network of the Compound Astronomical Low-cost Low Frequency for Transportable Observatory (e-Callisto), aims in analyzing the trend of type II bursts in general and provides a detailed investigation on the origin of the analyzed high-frequency type II bursts. The data used are from 2010-2019. We were motivated to use the CALLISTO ground based spectrometer data as a locally installed instrument, to check its capacity in providing radio burst data compared to other ground based spectrometers. In this article, bandwidth, duration, starting frequency, and drift rate of type II bursts are measured, to investigate their association with CMEs and/or solar flares.

In section 2 and section 3, we discussed about the observational data and method, respectively. In section 4, we present the data analysis and results. The summary and conclusions of the article is described in section 5.

## 2. Observations

### 2.1. Radio observations

The present study executes a statistical analysis of 51 high starting frequency (150 MHz-450 MHz) type II bursts observed in the metric wavelengths using data obtained from the e-Callisto network to examine their origin. The sample of events was observed for nine years in SC 24 (from 2010 to

2019). To begin with, we have identified the Type II bursts using the National Oceanic and Atmospheric Administration (NOAA) solar and geophysical reports<sup>1</sup>. From that list, we further identified the HF type II observed by different CALLISTO stations. For radio data, we used the spectral data obtained using various observatories of the e-Callisto network<sup>2</sup>, including the CALLISTO station in Rwanda<sup>3</sup>. The CALLISTO spectrometer is a new concept for solar radio observations, designed, developed, and distributed by Christian Monstein (Benz et al., 2005). CALLISTO is a low-frequency radio spectrometer used to monitor metric and decametric radio bursts and has been installed at different longitudes, enabling monitoring the radio emissions  $24 \times 7$ . All CALLISTO spectrometers constitute the e-Callisto network for data transfer online. More than 152 stations are in operation, and 55 of them provide real-time data to the server (one frame every 15 minutes) located at the University of Applied Sciences (FHNW) in Brugg/Windisch, Switzerland.

In Figure 1, panel (a) shows a processed dynamic spectrum of a low starting frequency burst observed by CALLISTO station in RWANDA on August 22, 2015, at  $\sim 06:52-06:58$  UT<sup>4</sup>. It was processed to remove: i) the radio frequency interferences (RFIs); ii) the background using median subtraction. This is a typical type II radio burst with a band-splitting of fundamental emission (Roberts, 1959) in the frequency range 73 MHz-44 MHz. Panel (b) shows the dynamic spectrum of an HF type II burst obtained from CALLISTO ALMATY station on November 04, 2015, during  $\sim 03:25-03:27$  UT<sup>5</sup>. Note that harmonic lane of type II burst starts at  $\sim 440$  MHz. The detailed analysis of the event is presented in Section 3.

## 2.2. White-light and EUV observations

The white-light CMEs data used in this study are obtained with the LASCO onboard SOHO (Brueckner et al., 1995) and the Cor1 and Cor2 coronagraphs from the Sun-Earth Connection Coronal and Heliospheric Investigation (SECCHI; Howard et al. (2008)) onboard the Solar Terrestrial Relations Observatory (STEREO). We extensively used the Coordinated Data Analysis Workshop (CDAW) CME database<sup>6</sup>, which is an online CME catalogue (Yashiro et al., 2004, 2008;

---

<sup>1</sup>[ftp://ftp.ngdc.noaa.gov/STP/swpc\\_products/](ftp://ftp.ngdc.noaa.gov/STP/swpc_products/)

<sup>2</sup><http://www.e-callisto.org/>

<sup>3</sup>[http://www.e-callisto.org/StatusReports/status\\_83\\_V01.pdf](http://www.e-callisto.org/StatusReports/status_83_V01.pdf)

<sup>4</sup>[http://soleil.i4ds.ch/solarradio/qkl/2015/08/22/RWANDA\\_20150822\\_064503\\_59.fit.gz.png](http://soleil.i4ds.ch/solarradio/qkl/2015/08/22/RWANDA_20150822_064503_59.fit.gz.png)

<sup>5</sup>[http://soleil.i4ds.ch/solarradio/qkl/2015/11/04/ALMATY\\_20151104\\_031500\\_59.fit.gz.png](http://soleil.i4ds.ch/solarradio/qkl/2015/11/04/ALMATY_20151104_031500_59.fit.gz.png)

<sup>6</sup><https://cdaw.gsfc.nasa.gov/>

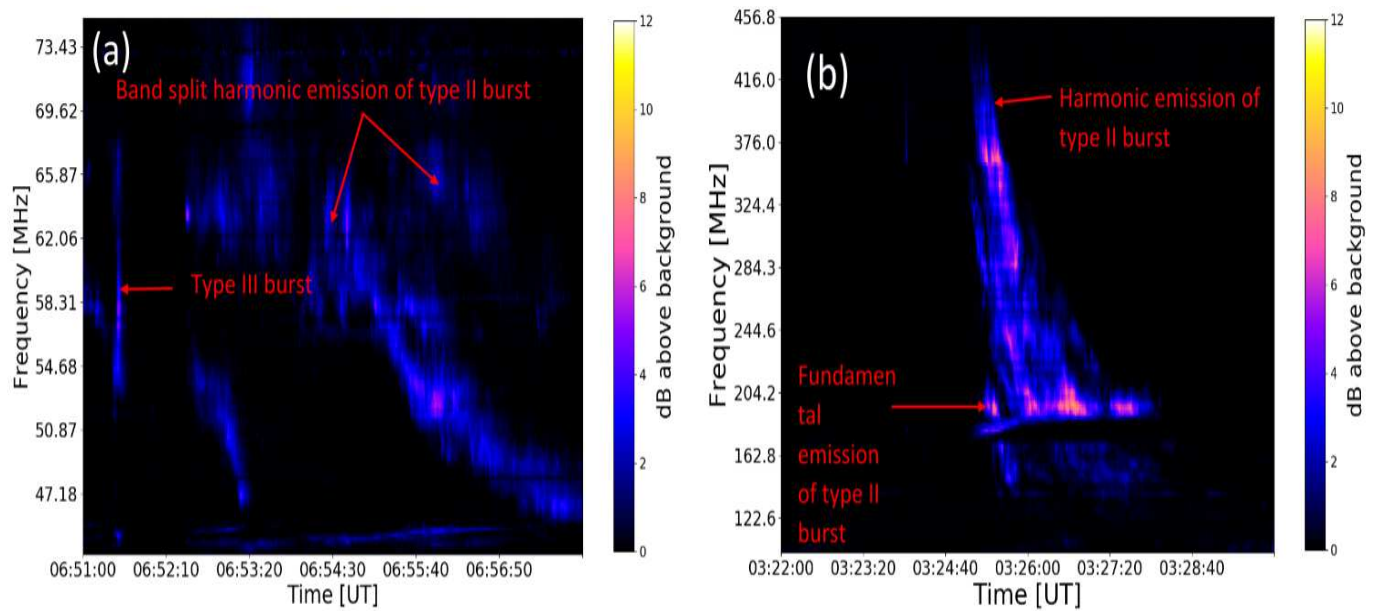


Figure 1: (a) The processed low-frequency type II burst dynamic spectrum was observed by CALLISTO RWANDA station on August 22, 2015. Its drift rate is  $-0.08$  MHz/s. It was associated with an M1.2 flare located near the solar disk (N15E20). Its associated CME has an average shock speed of 547 km/s. (b) shows the high frequency ( $\geq 150$  MHz) burst observed by CALLISTO ALMATY station on November 04, 2015. Its drift is higher ( $-0.83$  MHz/s) and consistent with its starting frequency. The associated M3.1 flare originates at N15W24 on the solar disk. The associated CME has an average speed of 272 km/s.

Gopalswamy et al., 2009b). The CMEs listed in this catalog use SOHO/LASCO white-light coronagraph data by manual detection of CMEs. We obtained information like CME linear speed within the LASCO field of view, estimated CME time, widths, and we accessed CME images and movies within STEREO. The link also guided the Geostationary Operational Environmental Satellite (GOES) to check the flare properties associated with the CMEs corresponding to the selected HF type II bursts, such as their onset time and classes. We also used observations at 171 Å/211 Å with the Atmospheric Imaging Assembly (AIA; Lemen et al., 2012) onboard the Solar Dynamics Observatory (SDO; Yashiro et al., 2020).

### 3. Method

#### 3.1. Identification of type II bursts

Type II bursts and their quality (ranging from 1 (poor) to 5 (excellent)) were first checked from the website of the space weather prediction center (SWPC<sup>7</sup>). The frequency range and observed timing were estimated from the dynamic spectra provided by CALLISTO spectrometers. Further, observationally derived parameters of HF type II bursts are used to characterize the properties of associated CMEs using the LASCO catalog. We considered the comparison of the time difference between the first appearance of the CME in the STEREO coronagraph/SDO and the observation of the fundamental band of the metric type II bursts to confirm their association (Claßen and Aurass, 2002). In this study, we considered 15 minutes of difference. However, for some events, the fundamental and harmonic band could not be distinguished easily.

#### 3.2. Derivation of CME speeds using SRBs physical parameters

The parameters obtained with radio observations, such as drift rate, can indicate CME-driven shock temporal evolution, as the type II bursts generally are associated with CME shock (Gopalswamy et al., 2010; Kumari et al., 2017a). The drift rate of type II radio burst is calculated by,

$$DR[\text{MHz/s}] = \frac{\Delta f[\text{MHz}]}{\Delta t[\text{s}]} = \frac{f_e - f_s}{t_e - t_s} \quad (1)$$

where, DR,  $f_s$ ,  $f_e$ ,  $t_s$  and  $t_e$  are the drift rate, start frequency, end frequency, start time and end time of the type II burst. The frequency cut-offs and time duration are in MHz and seconds, and

---

<sup>7</sup>[ftp://ftp.ngdc.noaa.gov/STP/swpc/\\_products/](ftp://ftp.ngdc.noaa.gov/STP/swpc/_products/)

the drift rate is expressed in MHz/s. There is a relationship between the drift rate of metric type II burst, the shock speed that produces the burst, and the density gradient in the solar corona (Gopalswamy, 2011). Therefore, the drift rate  $\frac{\Delta f}{\Delta t}$  at the observed frequency can be related to the speed of the source (Mann and Klassen, 2005; Aguilar-Rodriguez et al., 2005). The speed of the CME/CME shock can be estimated using the expression given by Gopalswamy et al. (2006); Gopalswamy (2011) as,

$$V[km/s] = -\frac{2r}{\alpha} \frac{1}{f[MHz]} \frac{\Delta f[MHz]}{\Delta t[s]} \quad (2)$$

where,  $f$  is the type II starting frequency or emission frequency,  $r$  is the shock height expressed in solar radii,  $R_s = 696000$  km and  $\alpha$  is the exponent describing density ( $n$ ) variation over the radial distance ( $n \sim r^{-\alpha}$ ). In this study, we used  $\alpha=7.56$ , which was previously derived by Gopalswamy et al. (2013) for metric type II bursts.

### 3.3. Measurement of CME shock heights at type II onset

We used contemporaneous data of extreme ultraviolet (EUV) solar data from the Solar Dynamic Observatory (SDO), white-light CME data from STEREO, and type II data from CALLISTO spectrographs. We did a case study on 05 October 2013 and 13 June 2010 HF type II bursts to validate the aforementioned method. We used this dataset as the CME evolution was clearly seen in the STEREO FOV. We took proper measures to minimize the projection effect due to the location of the source region. We used the leading edge and wave diameter methods. In the wave diameter method an approximately circular EUV or white-light disturbance is observed in the images, and a circle is fitted to the outermost part of the disturbance. The radius of the circle is then taken as the CME shock height. If the shock feature in the images is not clear in the leading edge method, the CME leading front height is taken as the height at which the type II burst (shock) forms. We have taken the CME height to be the same as the shock height and the type II burst height, as in Gopalswamy et al. (2013).



Table 1: Details of the events: Type II bursts, CMEs and Flares

SN	Type II <sup>1</sup> (UT)	fs <sup>2</sup> (MHz)	df/dt <sup>3</sup> (MHz/s)	CME <sup>4</sup> (UT)	$v_l$ <sup>5</sup> (km/s)	$v_d$ <sup>6</sup> (km/s)	$v_{II}$ <sup>7</sup> (km/s)	Width <sup>8</sup> (degrees)	r <sup>9</sup> (Rs)	Flare <sup>10</sup> UT	Loc <sup>11</sup>	Class <sup>12</sup>	r and $v_{II}$ <sup>13</sup> measurement method
1	20100612 01:00:00- 01:03:30	170	-0.28	01:06:04	486	579	673	119	1.91	01:30	N23W43	M6.0	LE
2	20100613 05:39:00-05:45:00	220	-0.25	05:36:08	320	245	522	16	1.17	05:40	S23W75	M1.0	LE
3	20101103 12:15:30-12:19:00	450	-0.47	12:16:08	241	258	511	66	1.34	12:10	S18E88	C9.2	LE
4	20110308 03:46:00- 03:51:00	160	-0.33	04:12:05	732	516.5	1370	260	1.36	03:37	S21W72	M1.5	LE
5	20110607 06:38:00- 06:38:45	160	-0.67	06:40:56	1255	1557.5	986	360	2.02	07:00	S21W54	M9.1	LE
6	20110828 04:20:00 - 04:24:00	160	-0.25	04:24:08	433	420	847	72	1.46	-	-	-	LE
7	20110906 01:47:00- 01:49:00	250	-0.83	01:50:31	782	1027	982	360	1.68	01:36	N14W07	M5.7	LE
8	20110906 22:19:00- 22:21:00	450	-1.66	22:20:00	575	971	1032	360	1.43	22:45	N14W16	X8.2	LE
9	20111001 09:07:00-09:11:00	170	-0.29	09:15:30	448	575	974	203	1.83	09:45	N10W06	M1.0	LE
10	20111114 09:24:00- 09:26:00	170	-0.41	09:25:30	553	666	880	10	1.50	09:50	N20W51	C9.0	LE
11	20120517 01:33:00 - 01:34:30	170	-0.88	01:48:05	1582	1811	2220	360	1.90	01:25	N13W87	M5.1	LE
12	20120603 17:50:00 - 17:55:00	195	-0.28	17:55:21	605	367.5	793	180	1.39	17:55	N16E38	M3.3	LE
13	20120607 20:03:00 - 20:09:00	180	-0.22	20:05:30	494	439	639	173	1.95	20:06	S19W05	M2.1	LE
14	20120608 03:08:00-03:15:00	211	-0.18	03:10:30	316	253	673	94	1.61	03:20	S09W21	M1.0	LE
15	20120702 05:10:00- 05:13:30	170	-0.19	06:00:04	251	276	626	90	1.34	06:00	N17E02	C8.0	LE
16	20120728 20:52:00 - 21:00:00	400	-0.41	20:55:30	420	287	504	360	1.52	20:56	S25E54	M6.1	LE
17	20120806 08:20:30 - 08:24:00	160	-0.14	08:36:06	242	285	520	56	1.77	08:35	S12E59	C5.9	LE
18	20121121 07:01:00- 07:09:00	360	-0.250	07:06:00	297	210	390	70	1.51	06:56	N06E10	M1.4	LE

19	20130113	08:40:00- 08:42:00	300	-1.08	08:48:05	696	829	929	46	1.25	09:10	N17W22	M9.1	LE
20	20130411	07:03:00 - 07:05:00	160	-0.50	07:10:00	861	834	1096	360	1.45	06:55	N10W01	M6.5	LE
21	20130502	05:07:00-05:13:30	170	-0.33	05:24:05	671	608	1186	99	1.70	05:30	N10W28	M1.0	WD
22	20130517	08:52:00-08:55:00	270	-0.97	08:50:27	1345	992	1183	360	1.50	08:43	N12E22	M3.2	LE
23	20131005	06:58:30- 07:00:00	170	-0.66	06:55:30	964	1229.5	1450	360	1.72	-	-	-	LE
24	20131011	07:11:00- 07:14:00	250	-0.94	07:12:07	1200	928	964	360	1.34	07:10	S08E20	C9.0	LE
25	20131025	08:00:30 - 08:09:00	240	-0.37	08:12:05	587	451	893	360	1.59	08:10	N06W24	C6.0	LE
26	20131107	03:40:00- 03:42:00	250	-0.41	04:05:31	373	486	526	69	1.61	03:34	S11E10	M2.3	WD
27	20131107	14:25:00-14:27:00	260	-0.50	14:45:00	411	443	626	360	1.25	15:17	S12E21	M2.4	LE
28	20131207	07:26:00 - 07:30:00	240	-0.5	07:36:05	1085	522	1276	360	1.36	07:35	S13W11	C2.0	LE
29	20131212	03:19:00- 03:22:00	150	-0.45	03:20:08	1002	806.5	1100	276	1.46	03:20	S23W46	C3.0	WD
30	20140106	07:47:00 - 07:49:30	160	-0.60	08:00:05	1402	1036	1579	360	1.50	07:30	S13W83	C2.1	LE
31	20140108	03:48:30-03:52:00	240	-0.57	03:48:09	643	560	535	108	1.28	03:39	N11W91	M3.6	LE
32	20140126	08:36:30- 08:38:00	150	-0.56	08:36:05	1088	1251	1368	255	1.82	09:00	S17E89	C3.1	LE
33	20140211	13:27:00 - 13:30:00	450	-1.10	13:48:05	330	711	851	208	1.58	13:50	S11E11	C9.0	LE
34	20140220	07:49:45-07:49:00	300	-1.55	07:45:57	948	1122.5	995	360	1.18	07:26	S14W81	M3.0	LE
35	20140306	09:27:00- 09:28:30	220	-0.55	09:30:53	252	635	476	56	1.38	06:30	N15W36	C3.0	LE
36	20140822	10:20:00- 10:21:30	170	-0.50	11:12:05	217	-	-	38	-	11:10	N10W07	C2.2	-
37	20140928	02:47:00-02:56:00	200	-0.18	02:48:09	215	232	493	60	1.40	02:48	S14E24	M8.0	WD
38	20141030	13:08:00-13:13:00	200	-0.23	13:08:00	285	330	541	112	1.56	12:37	S12W91	C2.9	LE
39	20141102	09:45:00-09:47:00	160	-0.33	10:00:06	461	605	555	≥ 168	1.45	09:20	S12W91	C4.5	LE
40	20150311	16:24:00-16:30:00	200	-0.19	17:00:05	240	224	638	74	1.28	16:11	S16E13	X2.1	WD
41	20150601	13:32:00-13:34:30	200	-0.53	13:36:00	748	654	715	360	1.34	-	-	-	LE

42	20150822 06:50:00-06:52:30	155	-0.30	07:12:00	547	641.5	601	360	1.80	06:39	S14E09	M1.2	LE
43	20151017 04:22:00- 04:26:00	165	-0.18	04:36:00	218	325	561	70	1.62	05:20	S10E33	C6.5	LE
44	20151104 03:24:00- 03:29:00	450	-0.83	04:00:04	272	–	–	64	–	04:00	N15W24	M3.1	–
45	20151104 12:03:00-12:08:00	410	-0.70	12:36:04	283	–	–	64	–	12:30	N05W04	M8.0	–
46	20160710 01:00:00-01:03:00	260	-0.44	01:05:30	368	461	534	101	1.48	00:53	N09E49	C8.6	LE
47	20170403 14:25:30- 14:28:30	350	-0.8	14:25:30	471	518	580	80	1.23	14:24:00	N15W76	M8.5	LE
48	20171018 05:38:00- 05:45:00	200	-0.53	05:40:00	1576	688	580	360	1.41	–	–	–	WD
49	20190421 04:46:00- 04:56:00	152	-0.26	04:48:00	463	794	565	274	1.43	–	–	–	LE
50	20190422 02:52:00- 03:00:00	162	-0.34	03:12:00	422	981.5	567	269	1.21	–	–	–	LE
51	20190506 05:12:00- 05:15:00	165	-0.51	05:20:30	239	1053	950	53	1.85	05:18	N09E47	M1.0	LE

---

<sup>2</sup> $f_s$  = Highest start frequency of type II bursts, which can be either fundamental and/or harmonic

<sup>3</sup> $df/dt$  = Drift rate

<sup>5</sup> $v_l$  = Average CME speed within LASCO FOV

<sup>6</sup> $v_d$  = CME shock speed derived using parameters from dynamic spectra

<sup>7</sup> $v_{II}$  = CME shock speed at type II onset

<sup>9</sup> $r$  = CME shock heights at type II onset

<sup>11</sup>Loc = Solar flare heliographic coordinates

<sup>1</sup>UT = Universal time

<sup>9</sup> $R_s$  = Solar radii

<sup>13</sup>LE = Leading Edge

<sup>13</sup>WD = Wave Diameter

## 4. Results and discussions

We prepared a list of HF type II bursts from SWPC event lists and their associated CMEs and flares from 2010-2019. Table 1 contains the list of these events. Columns (2 to 4) list the type II parameters such as type II onset and end times (duration), type II upper-frequency cut-off, and the drift rate of type II bursts. Columns (5 to 10) lists the associated CME characteristics such as the CME shock time, its average linear speed within LASCO FOV ( $v_l$ ), CME average speed derived using parameters estimated from the CALLISTO dynamic spectra ( $v_d$ ), the average CME shock speed at type II onset ( $v_{II}$ ), CME width and CME heights at type II onset ( $r$ ). Columns (11 to 13) list the flare onset time, flare location, and the flare class, respectively. The last column shows the measurement methods used to find the shock heights and CME speeds at type II onset.

### 4.1. Occurrence of high frequency type II bursts

From 2010 until 2019, the SWPC event list reported a total of 365 type II bursts. Out of these type II bursts, only 107 type II bursts were detected with an e-Callisto spectrometer. Among these 365 type II bursts, 84 ( $\sim 23\%$ ) are not associated with CMEs. Figure 2a shows the distribution of occurrence of type II bursts, type IIs associated with the CMEs, and type II bursts observed with the e-Callisto network per year from 2010-2019. Figure 2b shows the distribution of occurrence of all type II bursts, HF type II bursts, and HF type II bursts observed with the e-Callisto network per year in the same period. There is a total of 180 HF type II bursts reported. We selected 51 ( $\sim 28\%$ ) HF type II bursts observed with e-Callisto solar spectrometers. Some CALLISTO instruments cannot track the Sun, reducing potential observation time to about 4 hours per day. The CALLISTO in Rwanda falls in this category. Moreover, e-Callisto, in principle, can only detect the radio bursts which radiate in the design frequency range of CALLISTO, ranging between 45 MHz and 870 MHz, i.e., meter wavelength radio bursts. Also, It cannot see metric bursts behind the Sun, as they are formed at low heights. If the bursts continue to higher heights, they can be detected by space-borne instruments (deca-hectometric or kilometric bursts, also known as DH and km type II bursts). Results from this study indicate that all 51 HF type II bursts analyzed are associated with CMEs in agreement with previous studies by [Gopalswamy \(2006\)](#); [Ramesh et al. \(2012\)](#); [Cho et al. \(2013\)](#) who found that the formation of type II bursts in the low corona are explained by the CME-driven shock, the analysis considered different methods. Most of the type II bursts were reported in 2014, which was also the peak of solar cycle 24. Figure 2c shows the

distribution of X-ray flare class associated with the HF type II bursts observed with e-Callisto. Out of these shortlisted 51 radio bursts, 45 were accompanied by X-ray flares. Most of the HF type II bursts are associated with M ( $\sim 58\%$ ) and C ( $\sim 38\%$ ) class X-ray flares, respectively. Only ( $\sim 4\%$ ) HF type II bursts are associated with X class flares, and none of these bursts are accompanied by B class flares. Figure 2d shows the heliographic longitudes and latitudes of the flares associated with the type II bursts and it is found that all of them originate close to the equator (heliographic latitudes  $\pm 25^\circ$ ), the similar results were obtained by Mahender et al. (2020) who analyzed 426 type III bursts and found that most of them originate in heliographic coordinates  $\pm 23^\circ$ .

Figure 3a shows the variation of the starting frequency with the heliographic latitudes. Blue and red colors are indicating the northern and southern latitudes, respectively. Figure 3b illustrates the variation of the analyzed high-frequency type II bursts with the heliographic coordinates of the associated flares. The blue and red colors stand for the western and eastern longitudes. Due to the magnetic field connection governed by the Parker spirals and directivity of type II bursts (Gopalswamy et al., 2016; Sasikumar Raja and Ramesh, 2013; Mahender et al., 2020), presumably, we might have observed more number of type II bursts originated from the western longitude (27/45), with a high probability to produce a Solar Energetic Particle (SEP) event. The points above the dashed line in Figures a and b indicate the variation of the higher-starting-frequency ( $\geq 300$  MHz) bursts with the heliographic latitudes and longitudes, respectively. Similarly, 6/10 (60%) of the bursts originate from the western heliographic longitudes and range between  $-25^\circ$  and  $+25^\circ$  at the latitudes. In general, the analyzed high-frequency type II bursts are close to the disk center, similar to the previous study by Singh et al. (2019) on the analysis of type III using the statistical method.

#### 4.2. SEPs and the analyzed high starting frequency type II bursts

The same shock produces the type II radio bursts and the accelerated ions; thus, one would expect the association between type II bursts and SEP events (Kahler et al., 1984b; Cane et al., 1990). In this study, nine events out of 51 are accompanied by SEP events. Table 2 lists the 9 CMEs associated with the analyzed high starting frequency type II bursts accompanied by SEP enhancements. The table contains the following information: Type II date, starting frequency (MHz), the average speed of the associated CME obtained from the LASCO catalog list, CME speeds derived using type II parameters estimated from the dynamic spectra, CME speeds at type II onset, CME angular

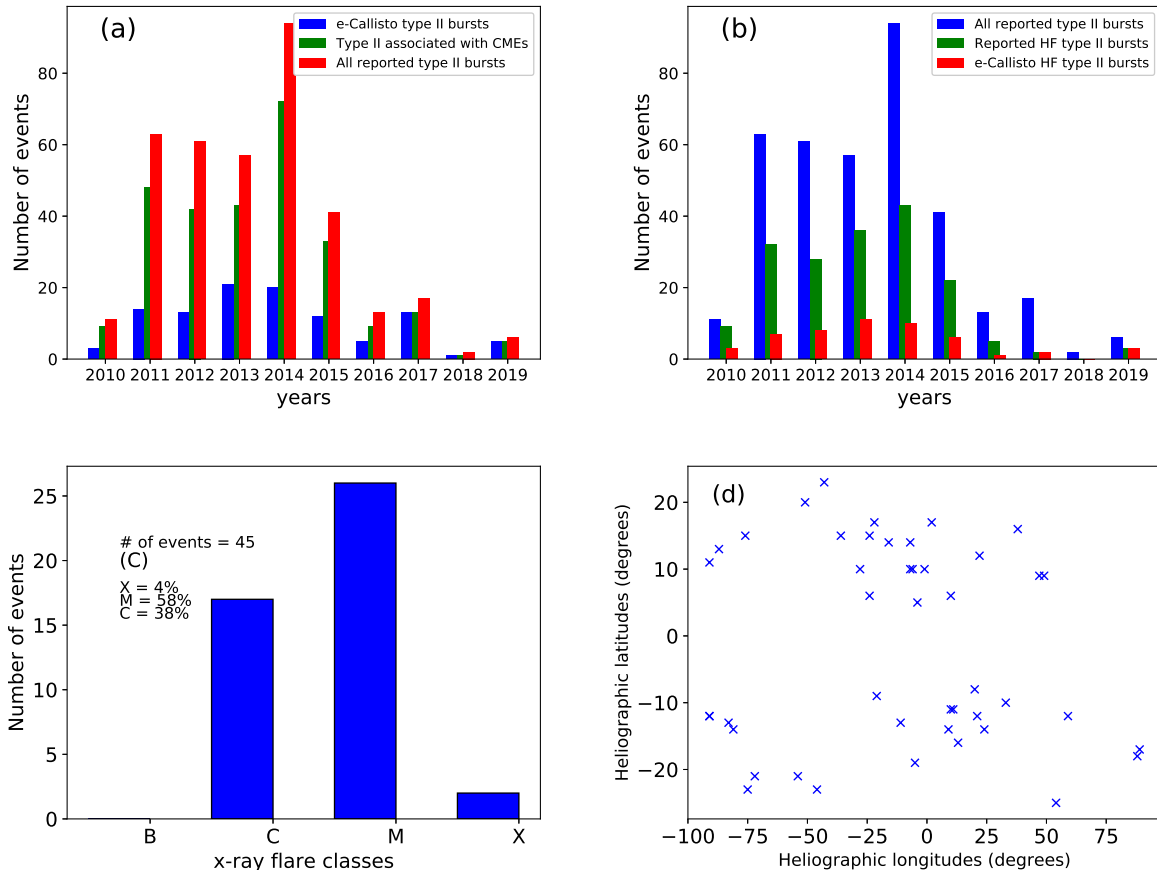


Figure 2: (a) Distribution of type II bursts, type IIs associated with the CMEs and type II bursts observed with e-Callisto network per year from 2010-2019 represented by ‘red’, ‘green’ and ‘blue’ colors, respectively. (b) type II bursts, HF type IIs and HF type II bursts observed with e-Callisto network per year from 2010-2019 represented by ‘blue’, ‘green’ and ‘red’ colors, respectively; (c) X-ray flares class associated with HF type II radio bursts; and (d) Heliographic longitude Vs heliographic latitude of flares associated with the high-frequency type II bursts.

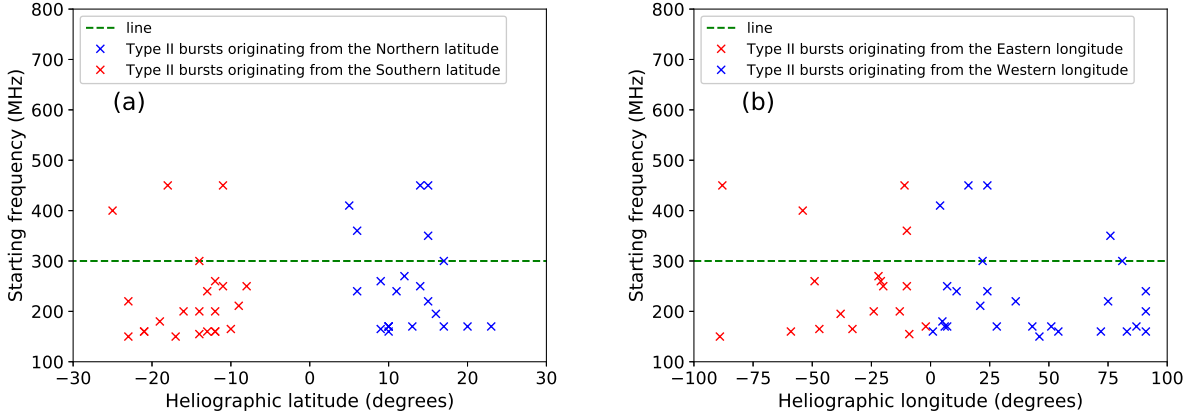


Figure 3: (a) The variation of the analyzed high frequency type II bursts with the heliographic latitude. (b) The variation of the analyzed high frequency type II bursts with the heliographic longitude. The green dashed lines on both Figures (3 a and b) indicate the selected events with higher-starting frequency ( $\geq 300$  MHz).

width, heliographic coordinates of the associated flare, the associated flare class, SEP intensity ( $I_p$  in pfu), and the approximate duration of the SEP event in days. The analysis found that 8/9 CME events accompanied by SEP events are fast, wide, and originate from the western hemisphere. Of the 9 events, 7 are associated with M class flare. The average speed at type II onset (1118 km/s) of the SEP- associated CMEs is around two times the average speed at type II onset of all analyzed CMEs. Among the 9 SEP-accompanied CMEs analyzed in this study, 5 are halo CMEs, 3 have widths greater than  $100^\circ$  except the 20131107 events originating from the Eastern hemisphere, which is having a width of  $69^\circ$ . The present study confirms the previous results (Gopalswamy et al., 2002; Gopalswamy, 2003). The Proton, Height-Time, X-ray (PHTX) plots of the SEP-accompanied events can be accessed on [https://cdaw.gsfc.nasa.gov/CME\\_list/daily\\_plots/sephtx/](https://cdaw.gsfc.nasa.gov/CME_list/daily_plots/sephtx/) and more information about the PHTX plots can be found in Gopalswamy et al. (2009c).

Table 2: Type II bursts associated with SEP events

SN	Type II	fs	$v_l$	$v_d$	$v_{II}$	Width	Loc	Flare	$Ip^a$	Dur ( <i>days</i> ) <sup>b</sup>
	Date	MHz	km/s	km/s	km/s	deg		Class		
1	20110308	160	732	516.5	1370	260	S21W72	M1.5	60	F
2	20120517	170	1582	1811	2220	360	N13W87	M5.1	120	F
3	20130411	160	861	834	1096	360	N10W01	M6.5	100	F
4	20130517	270	1345	992	1183	360	N12E22	M3.2	13	HiB
5	20131107	250	373	486	526	69	S11E10	M2.3	8	2
6	20140106	160	1402	1036	1579	360	S13W83	C2.1	60	F
7	20140108	240	643	560	535	108	N11W91	M3.6	> 1000	HiB and F
8	20140220	300	948	1122.5	995	360	S14W81	M3.0	12	2
9	20141102	160	461	605	555	$\succeq$ 168	S12W91	C4.5	10	F

<sup>1a</sup> Proton intensity in pfu (particle flux unit); 1 pfu = 1 particle per ( $cm^2$  s sr). <sup>b</sup> Approximate duration of the SEP events in days. F denotes events followed by other events, and HiB denotes events occurring during the elevated SEP background due to preceding events. For F and HiB, it is difficult to estimate the number of days of the SEP event.



#### 4.3. CME height and high-frequency type II burst onset

Type II burst starting frequency indicates the distance from the eruption center where the electrons start to accelerate. The high starting frequency corresponds to the shock formation closer to the Sun. Figure 4 (a) is the distribution of CME heights for all analyzed events. The mean and median are 1.50 and 1.49 Rs, respectively. Figure 4 (b) shows the distribution of the CME heights for the 42 limb events (measured using the leading edge method to avoid projection effects). The mean and median CME heliocentric distances are 1.53 and 1.50 Rs, respectively, at the onset of HF type II bursts. The CME heights obtained in this study looks smaller compared to the heights obtained in [Gopalswamy et al. \(2006\)](#) and comparable to the CME heights obtained by [Umuhire et al. \(2021\)](#) who analyzed 40 high starting frequency type II bursts and found the mean and median CME heights of 1.44 and 1.34 Rs. This study confirms the physical relationship between type II bursts and CMEs due to the similarity between type II bursts heights and associated CME leading edge heights. Figure 4 (c) is the distribution of CME widths associated with the high-frequency type II bursts analyzed in this study. It was found that the CMEs associated with the analyzed bursts are wide and energetic with the mean and median of  $201^\circ$  and  $175^\circ$  ([Gopalswamy et al., 2008](#)). Figure 4 (d) is the correlation between the average CME speed within LASCO field of view ( $v_l$ ) and the speed estimated using corona density model as shown in equation 2 ( $v_d$ ) for the 48 events for which the shock was identified. The correlation coefficient (cc) is  $\sim 0.72$ . By excluding the three outliers (in red), the cc improves to  $\sim 0.84$

#### 4.4. Estimation of CME speed

Table 1 shows various parameters related to the HF type II bursts selected for this study and the associated CMEs and flares. The linear speed of the CME leading edge ( $v_l$ ) ([Yashiro et al., 2004](#); [Gopalswamy et al., 2009a](#)) observed with SOHO/LASCO is listed in column 5. The shock speed  $v_d$  (in column 6) represents CME speed derived using the corona density model (see equation 2) from HF type II radio burst observations, and  $v_{II}$  is the CME shock speed at type II onset obtained by linearly fitting the height-time measurements within STEREO FOV at the first appearance of type II bursts. Figure 5a shows the distribution of CME speeds within LASCO FOV. The average and median linear speeds of the CMEs are  $\sim 627$  and  $\sim 490$  km/s, respectively. Figure 5b shows the distribution of linear speeds estimated using parameters of the HF type II radio bursts spectra provided by CALLISTO. The average and median linear speeds of the CMEs are  $\sim 665$  and  $\sim 600$  km/s, respectively. The slightly higher linear speed estimates in the case of later are because this

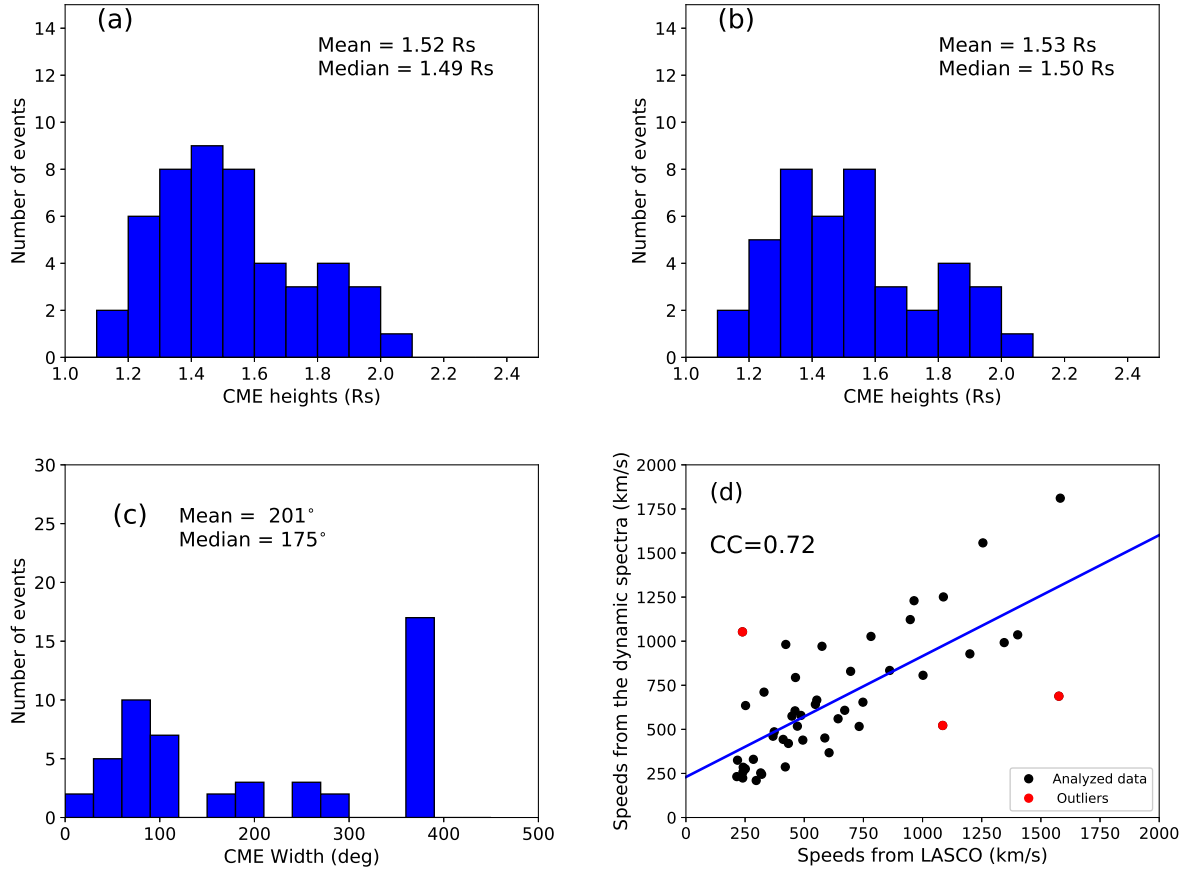


Figure 4: (a) The distribution of CME heights for all analyzed events, the mean and median are 1.52 and 1.49 Rs, respectively. (b) The distribution of CME heights at type II onset identified using the leading edge method. The mean and median are 1.53 and 1.50 Rs. (c) The distribution of CME widths associated with the analyzed type II bursts. (d) The correlation between the average CME speed within LASCO ( $v_l$ ) and the speed estimated using corona density model as shown in equation 2 ( $v_d$ ) for the 48 events for which the shock could be identified. The correlation coefficient (cc) is  $\sim 0.72$ . By excluding the three outliers (in red), the cc improves to  $\sim 0.84$ .

speed corresponds to the shock traveling ahead of the CME. Figure 5c is the distribution of CME shock speed at type II onset, the mean and median are  $\sim 799$  and  $\sim 693$  km/s, respectively. The average speed of CMEs at type II bursts onset is higher than the average CME speed within LASCO and comparable with the speed derived using the HF type II burst parameters estimated from the dynamic spectra. This is consistent with the CME shock formation confirming a study by Gopalswamy et al. (2008) who found that the average speeds of CMEs associated with metric type II bursts are 610 km/s. Moreover, the determined average speed of the shocks ahead of the CMEs at type II radio bursts onset is very close to the shock speed, which excites metric type II bursts in the ‘lower’ and ‘middle’ corona (i.e.,  $1.1 - 3 R_{\odot}$ ; Gosling et al. (1976)). Recently, Cunha-Silva et al. (2014) analyzed the properties of 4 type II bursts observed with CALLISTO spectrometer in Brazil and reported that the shock speed is in the range of 503 - 1259 km/s computed using Newkirk density model (Newkirk, 1961). Figure 5 (d) shows the correlation between  $v_d$  and  $v_{II}$ . The correlation coefficient (cc) is  $\sim 0.73$  and  $\sim 0.79$  by excluding the two outliers in red color. This high correlation coefficient values indicate that the speed derived from the coronal density model can be used as a proxy for estimating initial kinematics and dynamics of a CME in the lower corona in the absence of white-light observations (Kumari et al., 2017a, 2019). The radio data can also be used as a proxy for disk events, for which estimating the initial speed of CMEs is difficult due to projection effects.

#### 4.5. Case study

Event 1 (Type II burst observed on 13 June 2010): A HF type II burst was observed with the CALLISTO spectrometer at the Gauribidanur Radio Observatory (GRO)<sup>8</sup> on 13 June 2010 from 05:39-05:45 UT. Figure 6 (top panel) shows the dynamic spectra of the type II burst. The start frequency (harmonic emission) of the burst is  $\sim 190$  MHz. This type II burst had Fundamental, and Harmonic (F-H) bands and each of these two bands was further split into the split band. This radio burst had a drift rate of  $\sim 0.28$  MHz/s. It was associated with a CME with a linear speed of  $\sim 320$  km/s in SOHO/LASCO FOV. The estimated linear speed of the CME shock for the type II burst was found to be  $\sim 375$  km/s. During the onset of the type II burst, the CME must have been at the radial distance of  $\sim 1.17 R_s$ , measured using the wave diameter method (CME shock height is taken as the radius of the circle fitted to the outermost part of the disturbance, we assumed

---

<sup>8</sup><https://www.iiap.res.in/centers/radio>

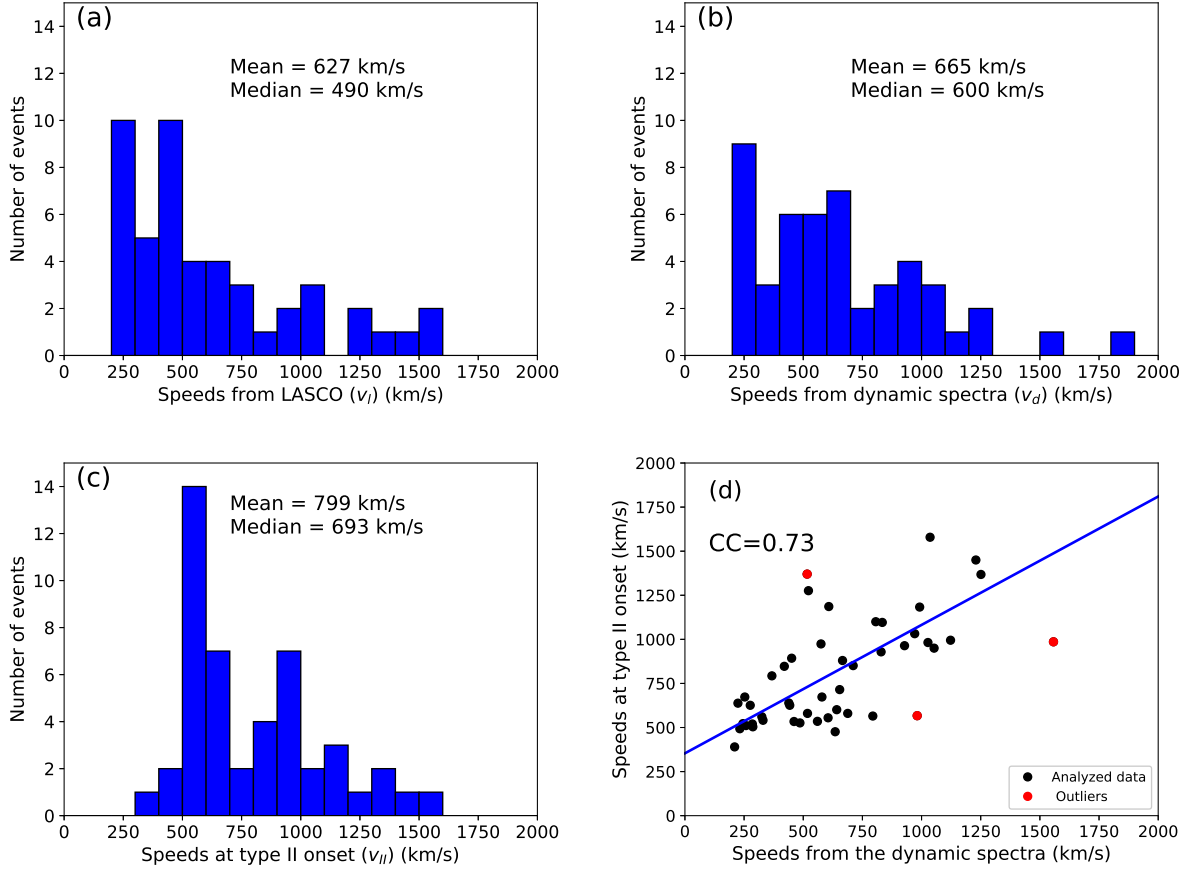


Figure 5: (a) Distribution of CME speeds within LASCFOV. The average and median CME speeds in the LASCFOV are  $\sim 627$  and  $\sim 490$  km/s, respectively. (b) Distribution of CME speeds from the dynamic spectra, the observed average and median are  $\sim 665$  and  $\sim 600$  km/s. (c) Distribution of CME speeds at type II onset, the mean and median are  $\sim 799$  and  $\sim 693$  km/s, respectively. The average CME speed at type II onset is higher compared to the speed in LASCFOV, which is consistent with the shock formation. (d) The correlation between the average CME speed at type II onset ( $v_{II}$ ) and the speed estimated using the corona density model ( $v_d$ ) for the 48 events for which the shock could be measured. The correlation coefficient ( $cc$ ) is  $\sim 0.73$ . By excluding the three outliers (in red), the  $cc$  improves to  $\sim 0.82$ . The 'blue' line shows a linear fit to the data.

that the disturbance expands spherically above the solar surface. The radius is shown by a pink line on the last image frame of CME in Figure 6 top panel. More details about the method are found in Gopalswamy et al. (2013)). The type II burst was associated with an M1.0 class X-ray flare that originated at S23W75 on the solar disk<sup>9</sup>. Figure 6 (top panel) also shows the CME in STEREO-A/EUVI and cor1 FOV. We used wave diameter method to estimate the CME shock height, where the CME shock height is taken as the radius of the sphere. Note that the event was detected by both STEREO and SDO spacecraft. We used STEREO/EUVI data for the height estimates and verified the same with SDO/AIA data.

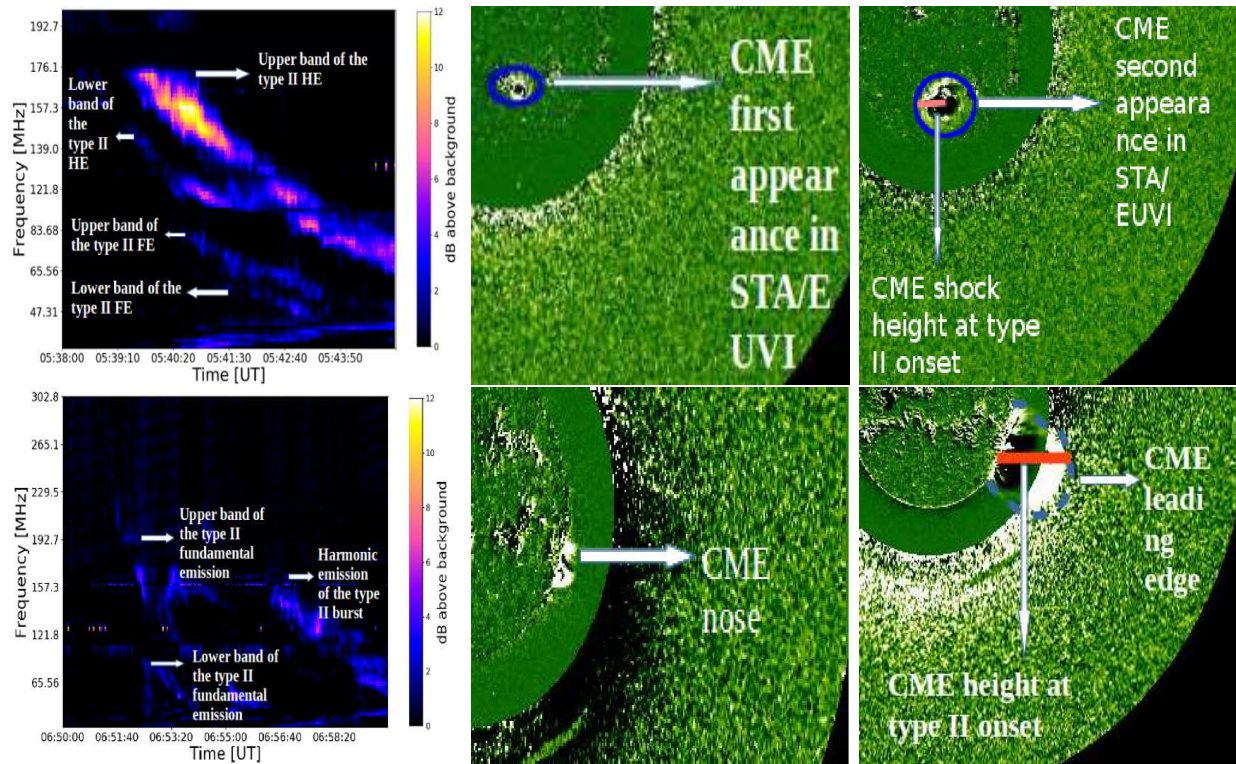


Figure 6: **Top panel:** The dynamic spectra of HF type II burst observed with the with the CALLISTO spectrometer at Gauribidanur Radio Observatory on 13 June, 2010 (note that FE and HE stands for fundamental and harmonic emissions). The start frequency of this busts is  $\sim 190$  MHz. Various features of this burst are marked on the spectra. The CME seen in STEREO FOV is also shown in this panel. The ‘blue’ circles represent the fitting of a circle to the EUV wave to measure the shock formation height. **Bottom panel:** The dynamic spectra of HF type II burst observed with the CALLISTO spectrometer at GRO on 05 October, 2013. The start frequency of this busts is  $\sim 240$  MHz. Various features of this burst are marked on the spectra. The CME seen in STEREO FOV is also shown in this panel.

<sup>9</sup><https://www.solarmonitor.org/?date=20100613>

Event 2 (Type II burst observed on 05 October 2013): Another HF type II burst was observed with the CALLISTO spectrometer at the same radio observatory on 05 October 2013 from 06:52-07:13 UT. Figure 6 (bottom panel) shows the dynamic spectra of the type II burst. The start frequency (harmonic emission) of the burst is  $\sim 240$  MHz. This type II burst had complex FH split bands. This radio burst had a drift rate of  $\sim 0.66$  MHz/s. This type II burst was associated with a CME with a linear speed of  $\sim 964$  km/s in SOHO/LASCO FOV. The estimated linear speed of the CME shock for the type II burst was found to be  $\sim 1006$  km/s. The measured CME shock height using the leading method (Gopalswamy et al., 2013) as found to be  $\sim 1.72$  Rs at 06:55:00 UT (the red line shows the shock height in Figure 6, bottom panel, last CME image frame). The type II burst was associated with a C2.0 class X-ray flare that originated at S03E43 on the solar disk<sup>10</sup>. Figure 6 (top panel) also shows the CME in STEREO-A/EUVI and cor1 FOV. We used the leading edge method as mentioned above to estimate the shock height.

## 5. Conclusion

In this study, we analyzed 51 high starting frequency type II solar radio bursts events which occurred during 2010-2019 detected by CALLISTO spectrometers. Ground-based CALLISTO instruments in metric wavelengths could detect 51 out of 180 high frequency (ranging between 150-450 MHz) type II bursts. We carried out a statistical study to check the origin of the analyzed high-frequency type II bursts. The analyzed CMEs associated with the 51 HF type II bursts are wide with the average and median widths of  $201^\circ$  and  $175^\circ$ , respectively. We used the corona density model as defined in a study by Gopalswamy et al. (2006); Gopalswamy (2011) to convert the parameters obtained with radio observations into the shock speed. The type II parameters derived from the dynamic spectra, such as the drift rates, are used in the empirical relations to derive the CME's shock speed associated with these radio bursts. The mean and median CME/shock speeds in the LASCO FOV, radio observations, and type II onset were  $\sim 627/665/799$  and  $\sim 490/600/693$  km/s, respectively. At type II onset, the CME shock speed was high enough to drive a shock ahead of a CME. In this work, the CME shock heights at type II onset were determined using either the leading edge method or wave diameter method depending on the CME location on the solar disk. The shock ahead of the analyzed CMEs was found within the heliocentric distances 1.17 to 2.02 Rs

---

<sup>10</sup><https://www.solarmonitor.org/?date=20131005>



with a mean and median of 1.52 and 1.49 Rs. The time difference of 15 minutes between the first appearance of the CME in the STEREO and the observation of the fundamental band of the metric type II was considered to confirm their association. Note that it was difficult to distinguish the type II burst fundamental and harmonic emissions for some cases. Therefore, the study analyzed particularly type II bursts with the starting frequency  $\geq$  to 300 MHz assuming harmonic emissions. The analysis found that all the analyzed HF type II bursts are due to CMEs, hence confirming the previous studies.

Of the 51 type II bursts 45 were associated with solar flares. We found that the flares associated with high-frequency type IIs have shorter rise time and duration and are stronger and more impulsive. Also, the analysis shows that more flares associated with the analyzed type II bursts originate from the active regions with heliographic latitude  $\pm 25^\circ$ . Also, the number of the bursts from the western longitudes is larger than that from the eastern longitude. Using the CME properties associated with the analyzed high starting frequency bursts such as speed, width, and solar source longitude, we found that 9/45 events are Solar Energetic Particle (SEP)-accompanied and 7/9 originate from the western hemisphere. This could be due to the magnetic connectivity between the observer located at the Earth and SEP source region. Similar results were previously obtained by [Gopalswamy \(2003\)](#); [Gopalswamy et al. \(2006, 2008\)](#) We also evaluated the performance of the coronal density model used to estimate the CMEs speed associated with type II bursts by comparing the estimated speed with the average CME shock speeds at type II onset using height-time measurements within STEREO FOV. The correlation is  $\sim 73\%$ .

As a case study, we analyzed two individual bursts with the Gauribidanur station of the e-Callisto network. Using the ground-based e-Callisto network with different longitudes, we can detect solar radio bursts within 24 hours a day, which serves as a warning of the associated solar transient, hence crucial for space weather studies ([Ndacyayisenga et al., 2021](#)). This analysis agrees with previous similar studies that higher frequency type II bursts can act as a proxy to estimate this eruption's early kinematics and dynamics near the Sun. Notably, the present study demonstrates the importance of using higher frequency type II bursts observed from the ground to monitor space weather prediction.

## Acknowledgements

The authors acknowledge the financial support from the Swedish International Development cooperation Agency (SIDA) through the International Science Program (ISP) to the University of Rwanda (UR-Swedish program) through the Rwanda Astrophysics, Space and Climate Science Research Group (RASCSRG). We thank the data centre of the e-Callisto network which is hosted by the FHNW, Institute for Data Science in Switzerland. Our sincere thanks goes to the providers of SOHO/LASCO-c2 CAW list and SWPC event list. One of the authors, A.K. acknowledges the ERC under the European Union's Horizon 2020 Research and Innovation Programme Project SolMAG 724391.

## References

- Aguilar-Rodriguez, E., Gopalswamy, N., MacDowall, R., Yashiro, S., Kaiser, M. L., Dec. 2005. A universal characteristic of type II radio bursts. *Journal of Geophysical Research (Space Physics)* 110, A12S08.
- Bale, S. D., Reiner, M. J., Bougeret, J. L., Kaiser, M. L., Krucker, S., Larson, D. E., Lin, R. P., Jan. 1999. The source region of an interplanetary type II radio burst. *Geophys. Res. Lett.* 26 (11), 1573–1576.
- Benz, A. O., Monstein, C., Meyer, H., Jan. 2005. Callisto A New Concept for Solar Radio Spectrometers. *Solar Phys.* 226, 143–151.
- Bougeret, J. L., Kaiser, M. L., Kellogg, P. J., Manning, R., Goetz, K., Monson, S. J., Monge, N., Friel, L., Meetre, C. A., Perche, C., Sitruk, L., Hoang, S., Feb. 1995. Waves: The Radio and Plasma Wave Investigation on the Wind Spacecraft. *Space Sci. Rev.* 71 (1-4), 231–263.
- Brueckner, G. E., Howard, R. A., Koomen, M. J., Korendyke, C. M., Michels, D. J., Moses, J. D., Socker, D. G., Dere, K. P., Lamy, P. L., Llebaria, A., Bout, M. V., Schwenn, R., Simnett, G. M., Bedford, D. K., Eyles, C. J., Dec. 1995. The Large Angle Spectroscopic Coronagraph (LASCO). *Solar Phys.* 162, 357–402.
- Cane, H. V., Reames, D. V., Feb. 1988. Some statistics of solar radio bursts of spectral types II and IV. *Astrophys. J.* 325, 901–904.



- Cane, H. V., Stone, R. G., Jul 1984. Type II solar radio bursts, interplanetary shocks, and energetic particle events. *The Astrophysical Journal* 282, 339–344.
- Cane, H. V., von Rosenvinge, T. T., McGuire, R. E., May 1990. Energetic particle observations at the Helios 1 Spacecraft of shocks associated with coronal mass ejections. *J. Geophys. Res.*95 (A5), 6575–6579.
- Carley, E. P., Baldovin, C., Benthem, P., Bisi, M. M., Fallows, R. A., Gallagher, P. T., Olberg, M., Rothkaehl, H., Vermeulen, R., Vilmer, N., Barnes, D., Jan. 2020. Radio observatories and instrumentation used in space weather science and operations. *Journal of Space Weather and Space Climate* 10, 7.
- Carley, E. P., Vilmer, N., Simões, P. J. A., Ó Fearraigh, B., Dec. 2017. Estimation of a coronal mass ejection magnetic field strength using radio observations of gyrosynchrotron radiation. *Astron. Astrophys.*608, A137.
- Cho, K.-S., Gopalswamy, N., Kwon, R.-Y., Kim, R.-S., Yashiro, S., Mar. 2013. A High-frequency Type II Solar Radio Burst Associated with the 2011 February 13 Coronal Mass Ejection. *apj* 765, 148.
- Claßen, H. T., Aurass, H., Mar. 2002. On the association between type II radio bursts and CMEs. *Astron. Astrophys.*384, 1098–1106.
- Cliver, E. W., Nitta, N. V., Thompson, B. J., Zhang, J., Nov. 2004. Coronal Shocks of November 1997 Revisited: The Cme Type II Timing Problem. *solphys* 225, 105–139.
- Cunha-Silva, R. D., Fernandes, F. C. R., Selhorst, C. L., Dec. 2014. Solar Type II Radio Bursts Recorded by the Compound Astronomical Low-Frequency Low-Cost Instrument for Spectroscopy in Transportable Observatories in Brazil. *solphys* 289, 4607–4620.
- Elgaroy, O., 1977. Solar noise storms by eo elgaroy.
- Fainberg, J., Stone, R. G., Nov. 1970. Type III Solar Radio Burst Storms Observed at Low Frequencies. *Solar Phys.*15, 222–233.
- Gary, D. E., Dulk, G. A., House, L. L., Illing, R., Wagner, W. J., Nov. 1985. The Type IV burst of 1980 June 29, 0233 UT - Harmonic plasma emission. *Astron. Astrophys.*152, 42–50.

- Gopalswamy, N., Jun. 2003. Solar and geospace connections of energetic particle events. *Geophys. Res. Lett.*30 (12), 8013.
- Gopalswamy, N., Nov. 2004a. A Global Picture of CMEs in the Inner Heliosphere. In: Poletto, G., Suess, S. T. (Eds.), *The Sun and the Heliosphere as an Integrated System*. Vol. 317 of *Astrophysics and Space Science Library*. p. 201.
- Gopalswamy, N., Sep. 2004b. Interplanetary Radio Bursts. In: Gary, D. E., Keller, C. U. (Eds.), *Astrophysics and Space Science Library*. Vol. 314 of *Astrophysics and Space Science Library*. p. 305.
- Gopalswamy, N., Oct. 2006. *Coronal Mass Ejections and Type II Radio Bursts*. Washington DC American Geophysical Union Geophysical Monograph Series 165, 207.
- Gopalswamy, N., Feb. 2010. The CME link to geomagnetic storms. In: Kosovichev, A. G., Andrei, A. H., Rozelot, J.-P. (Eds.), *Solar and Stellar Variability: Impact on Earth and Planets*. Vol. 264 of *IAU Symposium*. pp. 326–335.
- Gopalswamy, N., 2011. *Coronal Mass Ejections and Solar Radio Emissions*. *Planetary, Solar and Heliospheric Radio Emissions (PRE VII)*, 325–342.
- Gopalswamy, N., Akiyama, S., Mäkelä, P., Yashiro, S., Cairns, I. H., May 2016. On the Directivity of Low-Frequency Type IV Radio Bursts. arXiv e-prints, arXiv:1605.02223.
- Gopalswamy, N., Kaiser, M. L., Lepping, R. P., Kahler, S. W., Ogilvie, K., Berdichevsky, D., Kondo, T., Isobe, T., Akioka, M., Jan. 1998. Origin of coronal and interplanetary shocks - A new look with WIND spacecraft data. *Jgr* 103, 307.
- Gopalswamy, N., Lara, A., Kaiser, M. L., Bougeret, J.-L., Nov. 2001. Near-Sun and near-Earth manifestations of solar eruptions. *J. Geophys. Res.*106, 25261–25278.
- Gopalswamy, N., Mäkelä, P., Yashiro, S., Jan. 2019. A Catalog of Type II radio bursts observed by Wind/WAVES and their Statistical Properties. *Sun and Geosphere* 14, 111–121.
- Gopalswamy, N., Thompson, W. T., Davila, J. M., Kaiser, M. L., Yashiro, S., Mäkelä, P., Michalek, G., Bougeret, J.-L., Howard, R. A., Oct. 2009a. Relation Between Type II Bursts and CMEs Inferred from STEREO Observations. *Solar Phys.*259, 227–254.

- Gopalswamy, N., Xie, H., Mäkelä, P., Akiyama, S., Yashiro, S., Kaiser, M. L., Howard, R. A., Bougeret, J.-L., Feb. 2010. Interplanetary Shocks Lacking Type II Radio Bursts. *Astrophys. J.* 710, 1111–1126.
- Gopalswamy, N., Xie, H., Mäkelä, P., Yashiro, S., Akiyama, S., Uddin, W., Srivastava, A. K., Joshi, N. C., Chandra, R., Manoharan, P. K., Mahalakshmi, K., Dwivedi, V. C., Jain, R., Awasthi, A. K., Nitta, N. V., Aschwanden, M. J., Choudhary, D. P., Jun. 2013. Height of shock formation in the solar corona inferred from observations of type II radio bursts and coronal mass ejections. *Advances in Space Research* 51, 1981–1989.
- Gopalswamy, N., Yashiro, S., Akiyama, S., Mäkelä, P., Xie, H., Kaiser, M. L., Howard, R. A., Bougeret, J. L., Oct. 2008. Coronal mass ejections, type II radio bursts, and solar energetic particle events in the SOHO era. *Annales Geophysicae* 26 (10), 3033–3047.
- Gopalswamy, N., Yashiro, S., Kaiser, M., Bougeret, J.-L., Aug. 2006. Solar Energetic Particles and CME-driven Shocks. In: IAU Joint Discussion. Vol. 1 of IAU Joint Discussion.
- Gopalswamy, N., Yashiro, S., Michalek, G., Kaiser, M. L., Howard, R. A., Leske, R., von Roseninge, T., Reames, D. V., Sep. 2003. Effect of CME Interactions on the Production of Solar Energetic Particles. In: Velli, M., Bruno, R., Malara, F., Bucci, B. (Eds.), *Solar Wind Ten*. Vol. 679 of American Institute of Physics Conference Series. pp. 608–611.
- Gopalswamy, N., Yashiro, S., Michalek, G., Kaiser, M. L., Howard, R. A., Reames, D. V., Leske, R., von Roseninge, T., Jun. 2002. Interacting Coronal Mass Ejections and Solar Energetic Particles. *Astrophys. J. Lett.* 572 (1), L103–L107.
- Gopalswamy, N., Yashiro, S., Michalek, G., Stenborg, G., Vourlidas, A., Freeland, S., Howard, R., Apr. 2009b. The SOHO/LASCO CME Catalog. *Earth Moon and Planets* 104 (1-4), 295–313.
- Gopalswamy, N., Yashiro, S., Michalek, G., Stenborg, G., Vourlidas, A., Freeland, S., Howard, R., Apr. 2009c. The SOHO/LASCO CME Catalog. *Earth Moon and Planets* 104 (1-4), 295–313.
- Gosling, J. T., Hildner, E., MacQueen, R. M., Munro, R. H., Poland, A. I., Ross, C. L., Jun. 1976. The speeds of coronal mass ejection events. *solphys* 48, 389–397.
- Howard, R. A., Moses, J. D., Vourlidas, A., Newmark, J. S., Socker, D. G., Plunkett, S. P., Korendyke, C. M., Cook, J. W., Hurley, A., Davila, J. M., Thompson, W. T., St Cyr, O. C.,

- Mentzell, E., Mehalick, K., Lemen, J. R., Wuelser, J. P., Duncan, D. W., Tarbell, T. D., Wolfson, C. J., Moore, A., Harrison, R. A., Waltham, N. R., Lang, J., Davis, C. J., Eyles, C. J., Mapson-Menard, H., Simnett, G. M., Halain, J. P., Defise, J. M., Mazy, E., Rochus, P., Mercier, R., Ravet, M. F., Delmotte, F., Auchere, F., Delaboudiniere, J. P., Bothmer, V., Deutsch, W., Wang, D., Rich, N., Cooper, S., Stephens, V., Maahs, G., Baugh, R., McMullin, D., Carter, T., Apr. 2008. Sun Earth Connection Coronal and Heliospheric Investigation (SECCHI). *Space Sci. Rev.*136, 67–115.
- Kahler, S. W., Sheeley, N. R., J., Howard, R. A., Michels, D. J., Koomen, M. J., McGuire, R. E., von Roseninge, T. T., Reames, D. V., Nov. 1984a. Associations beteen coronal mass ejections and solar energetic proton events. *J. Geophys. Res.*89 (A11), 9683–9694.
- Kahler, S. W., Sheeley, N. R., J., Howard, R. A., Michels, D. J., Koomen, M. J., McGuire, R. E., von Roseninge, T. T., Reames, D. V., Nov. 1984b. Associations beteen coronal mass ejections and solar energetic proton events. *J. Geophys. Res.*89 (A11), 9683–9694.
- Krupar, V., Magdalenić, J., Eastwood, J. P., Gopalswamy, N., Kruparova, O., Szabo, A., Nĕmec, F., Sep. 2019. Statistical Survey of Coronal Mass Ejections and Interplanetary Type II Bursts. *Astrophys. J.*882 (2), 92.
- Kumari, A., Morosan, D. E., Kilpua, E. K. J., Jan. 2021. On the Occurrence of Type IV Solar Radio Bursts in Solar Cycle 24 and Their Association with Coronal Mass Ejections. *Astrophys. J.*906 (2), 79.
- Kumari, A., Ramesh, R., Kathiravan, C., Gopalswamy, N., Jul. 2017a. New Evidence for a Coronal Mass Ejection-driven High Frequency Type II Burst near the Sun. *Astrophys. J.*843, 10.
- Kumari, A., Ramesh, R., Kathiravan, C., Wang, T. J., Dec 2017b. Addendum to: Strength of the Solar Coronal Magnetic Field - A Comparison of Independent Estimates Using Contemporaneous Radio and White-Light Observations. *Solar Physics* 292 (12), 177.
- Kumari, A., Ramesh, R., Kathiravan, C., Wang, T. J., Nov 2017c. Strength of the Solar Coronal Magnetic Field - A Comparison of Independent Estimates Using Contemporaneous Radio and White-Light Observations. *Solar Physics* 292 (11), 161.

- Kumari, A., Ramesh, R., Kathiravan, C., Wang, T. J., Gopalswamy, N., Aug 2019. Direct Estimates of the Solar Coronal Magnetic Field Using Contemporaneous Extreme-ultraviolet, Radio, and White-light Observations. *The Astrophysical Journal* 881 (1), 24.
- Lara, A., Gopalswamy, N., Nunes, S., Muñoz, G., Yashiro, S., Jun. 2003. A statistical study of CMEs associated with metric type II bursts. *Geophys. Res. Lett.*30 (12), 8016.
- Lemen, J. R., Title, A. M., Akin, D. J., Boerner, P. F., Chou, C., Drake, J. F., Duncan, D. W., Edwards, C. G., Jan. 2012. The Atmospheric Imaging Assembly (AIA) on the Solar Dynamics Observatory (SDO). *Solar Phys.*275, 17.
- MacQueen, R. M., Jul. 1980. Coronal transients - A summary. *Philosophical Transactions of the Royal Society of London Series A* 297, 605–620.
- Magdaleníć, J., Marqué, C., Zhukov, A. N., Vršnak, B., Veronig, A., Feb. 2012. Flare-generated Type II Burst without Associated Coronal Mass Ejection. *Astrophys. J.*746 (2), 152.
- Mahender, A., Sasikumar Raja, K., Ramesh, R., Panditi, V., Monstein, C., Ganji, Y., Nov. 2020. A Statistical Study of Low-Frequency Solar Radio Type III Bursts. *Solar Phys.*295 (11), 153.
- Majumdar, S., Tadepalli, S. P., Maity, S. S., Deshpande, K., Kumari, A., Patel, R., Gopalswamy, N., Apr. 2021. Imaging and Spectral Observations of a Type-II Radio Burst Revealing the Section of the CME-Driven Shock That Accelerates Electrons. *Solar Phys.*296 (4), 62.
- Makela, P. A., Gopalswamy, N., Yashiro, S., Dec. 2013. The Radial Speed - Expansion Speed Relation for Earth-Directed CMEs. In: *AGU Fall Meeting Abstracts*. Vol. 2013. pp. SH31B–2033.
- Mann, G., Classen, T., Aurass, H., Mar. 1995. Characteristics of coronal shock waves and solar type II radio bursts. *Astron. Astrophys.*295, 775.
- Mann, G., Klassen, A., Oct. 2005. Electron beams generated by shock waves in the solar corona. *Astrophysical journal* 441, 319–326.
- Maxwell, A., Thompson, A. R., Jan. 1962. Spectral Observations of Solar Radio Bursts. II. Slow-Drift Bursts and Coronal Streamers. *Geophysical research* 135, 138.

- Mercier, C., Subramanian, P., Chambe, G., Janardhan, P., Apr. 2015. The structure of solar radio noise storms. *Astron. Astrophys.*576, 136.
- Morosan, D., Räsänen, E., Kilpua, E., Magdalenic, J., Lynch, B., Kumari, A., Pomoell, J., Palmroth, M., Oct. 2020. Electron acceleration and radio emission following the early interaction of two coronal mass ejections. *Astron. Astrophys.*A151 (9), 134.
- Morosan, D. E., Kumari, A., Kilpua, E. K. J., Hamini, A., Mar. 2021. Moving solar radio bursts and their association with coronal mass ejections. *Astron. Astrophys.*647, L12.
- Mujiber Rahman, A., Umapathy, S., Shanmugaraju, A., Moon, Y. J., Aug. 2012. Solar and interplanetary parameters of CMEs with and without type II radio bursts. *Advances in Space Research* 50 (4), 516–525.
- Ndacyayisenga, T., Uwamahoro, J., Sasikumar Raja, K., Monstein, C., Feb 2021. A statistical study of solar radio type iii bursts and space weather implication. *Advances in Space Research* 67 (4), 1425–1435.  
URL <http://dx.doi.org/10.1016/j.asr.2020.11.022>
- Newkirk, Jr., G., May 1961. The Solar Corona in Active Regions and the Thermal Origin of the Slowly Varying Component of Solar Radio Radiation. *Geophysical journal* 133, 983.
- Ramesh, R., Kathiravan, C., Satya Narayanan, A., Dec. 2004. Seismology of the solar corona through observations of metric type IV radio burst emission. *Asian Journal of Physics* 13, 277–284.
- Ramesh, R., Lakshmi, M. A., Kathiravan, C., Gopalswamy, N., Umapathy, S., Jun. 2012. The Location of Solar Metric Type II Radio Bursts with Respect to the Associated Coronal Mass Ejections. *Geophysical research* 752, 107.
- Ramesh, R., Sasikumar Raja, K., Kathiravan, C., Narayanan, A. S., Jan. 2013. Low-frequency Radio Observations of Picoflare Category Energy Releases in the Solar Atmosphere. *Astrophys. J.*762 (2), 89.
- Ratcliffe, H., Kontar, E. P., Reid, H. A. S., Dec. 2014. Large-scale simulations of solar type III radio bursts: flux density, drift rate, duration, and bandwidth. *Astron. Astrophys.*572, A111.

- Reiner, M. J., Karlický, M., Jiříčka, K., Aurass, H., Mann, G., Kaiser, M. L., Feb. 2000. On the Solar Origin of Complex Type III-like Radio Bursts Observed at and below 1 MHz. *Astrophys. J.*530, 1049–1060.
- Roberts, J. A., Dec. 1959. Solar Radio Bursts of Spectral Type II. *Australian Journal of Physics* 12, 327.
- Sasikumar Raja, K., Ramesh, R., Sep. 2013. Low-frequency Observations of Transient Quasi-periodic Radio Emission from the Solar Atmosphere. *Astrophys. J.*775 (1), 38.
- Sasikumar Raja, K., Ramesh, R., Hariharan, K., Kathiravan, C., Wang, T. J., Nov. 2014. An Estimate of the Magnetic Field Strength Associated with a Solar Coronal Mass Ejection from Low Frequency Radio Observations. *Astrophys. J.*796 (1), 56.
- Schmidt, J. M., Cairns, I. H., Lobzin, V. V., Aug. 2014. The solar type II radio bursts of 7 March 2012: Detailed simulation analyses. *Journal of Geophysical Research (Space Physics)* 119, 6042–6061.
- Shanmugaraju, A., Lawrance, M. B., Moon, Y., Lee, J.-O., Suresh, K., 2017. Heights of coronal mass ejections and shocks inferred from metric and dh type ii radio bursts. *Solar Physics* 292 (9), 136.
- Shanmugaraju, A., Moon, Y. J., Vrsnak, B., Feb. 2009. Type II Radio Bursts with High and Low Starting Frequencies. *Solar Phys.*254 (2), 297–310.
- Singh, D., Sasikumar Raja, K., Subramanian, P., Ramesh, R., Monstein, C., Aug. 2019. Automated Detection of Solar Radio Bursts Using a Statistical Method. *Solar Phys.*294 (8), 112.
- Stewart, R., et al., 1965. Solar radio bursts of spectral type v. *Australian Journal of Physics* 18 (2), 143–166.
- Su, W., Cheng, X., Ding, M. D., Chen, P. F., Sun, J. Q., may 2015. A TYPE II RADIO BURST WITHOUT a CORONAL MASS EJECTION. *The Astrophysical Journal* 804 (2), 88.  
URL <https://doi.org/10.1088%2F0004-637x%2F804%2F2%2F88>
- Suzuki, S., Dulk, G. A., 1985. Bursts of Type III and Type V. pp. 289–332.

- Umuhire, A. C., Gopalswamy, N., Uwamahoro, J., Akiyama, S., Yashiro, S., Mäkelä, P., Jan. 2021. Properties of High-Frequency Type II Radio Bursts and Their Relation to the Associated Coronal Mass Ejections. *Solar Phys.*296 (1), 27.
- Vasanth, V., Umopathy, S., Jan. 2013. A Statistical Study on DH CMEs and Its Geoeffectiveness. *ISRN Astronomy and Astrophysics 2013*, 1–13.
- Vrsnak, B., Ruzdjak, V., Zlobec, P., Aurass, H., May 1995. Ignition of MHD Shocks Associated with Solar Flares. *Solar Phys.*158 (2), 331–351.
- Yashiro, S., Gopalswamy, N., Akiyama, S., Mäkelä, P. A., Sep. 2020. A catalog of prominence eruptions detected automatically in the SDO/AIA 304 Å images. *Journal of Atmospheric and Solar-Terrestrial Physics* 205, 105324.
- Yashiro, S., Gopalswamy, N., Michalek, G., St. Cyr, O. C., Plunkett, S. P., Rich, N. B., Howard, R. A., Jul. 2004. A catalog of white light coronal mass ejections observed by the SOHO spacecraft. *Journal of Geophysical Research (Space Physics)* 109 (A7), A07105.
- Yashiro, S., Michalek, G., Gopalswamy, N., Oct. 2008. A comparison of coronal mass ejections identified by manual and automatic methods. *Annales Geophysicae* 26 (10), 3103–3112.
- Zlotnik, E. Y., Klassen, A., Aurass, H., Klein, K.-L., Mann, G., Jan. 1998. Interpretation of harmonic structure in solar type II radio bursts. *Radiophysics and Quantum Electronics* 41, 39–52.